IEEE Access
Multidisciplinary | Rapid Review | Open Access Journal

Received January 25, 2021, accepted February 8, 2021, date of publication February 18, 2021, date of current version March 1, 2021.

Digital Object Identifier 10.1109/ACCESS.2021.3060104

An Accurate Time-Based MPPT Circuit With Two-Period Tracking Algorithm and Convergence Range Averaging Technique for IoT Applications

VAN-THAI DANG, (Student Member, IEEE), MYEONG-GYU YANG, (Student Member, IEEE), YONG SHIM, (Member, IEEE), WOOJOO LEE, (Member, IEEE), AND KWANG-HYUN BAEK, (Senior Member, IEEE)

School of Electrical and Electronics Engineering, Chung-Ang University, Seoul 06974, South Korea

Corresponding author: Kwang-Hyun Baek (kbaek@cau.ac.kr)

This work was supported in part by the Chung-Ang University Young Scientist Scholarship (CAYSS) in 2018, in part by the Ministry of Trade, Industry and Energy (MOTIE) under Project 10080622, and in part by the Korea Semiconductor Research Consortium (KSRC) Support Program for the Development of the Future Semiconductor Device.

ABSTRACT This article proposes a highly efficient Time-Based Maximum-Power-Point-Tracking (TB-MPPT) integrated-circuit. Conventional TB-MPPT circuit shows unstable status (oscillation) near the Maximum Power Point (MPP), which causes the degradation of the overall power tracking efficiency. To overcome this critical issue, the proposed circuit separates the tracking operation into two periods, and it utilizes convergence range averaging technique with an adaptive perturbation step according to each control signal to accurately extract the current power level without oscillation problem. This work is fabricated in 180 nm CMOS process to demonstrate advantages of the proposed scheme. With 0.47V 12mW Photovoltaic (PV) cell, the measurement results show 94.2% of MPPT efficiency and 91.6% of power conversion efficiency (PCE). It occupies silicon chip area of 1.69 mm^2.

INDEX TERMS Convergence range averaging technique, dc-dc converter, energy harvesting system, time-based MPPT, two-period tracking algorithm.

I. INTRODUCTION

Most low-power IoT systems such as wearable biosensors and biometric devices are battery powered, and the batteries used in these systems typically contain only a small amount of limited energy due to the requirement for the small size of the target application. Therefore, periodic recharging is essential [1], [2], and this recharging is mainly performed through energy harvesting sources which can supply electronic circuits for an almost infinite lifetime. In addition, because energy harvesting sources can be placed close to the device, transmission losses caused by long cables can also be eliminated. Because of these advantages, studies on numerous energy harvesting sources including Photovoltaic (PV) cells [1], [3]–[13], TEG [14], and methods of using vibration [15] or RF signals [16], [17] have been discussed in the literature. Among these, PV cells is one of the most promising candidates that can be used in IoT systems due to its low cost and high-power density. Fig. 1 shows a simplified block diagram of an energy harvesting system (EHS) with PV cells. The energy collected from the PV cells is converted to the appropriate voltage and current values through a DC-DC converter in the Power Management Block (PMB) and then provided to the loads such as ADCs, sensors, and DSP circuits in target systems. One of the elements that plays a very important role in PMB is the Maximum-Power-Tracking-Point (MPPT) circuit. Since Maximum Power Point (MPP) can vary with irradiance and temperature, the MPPT circuit is

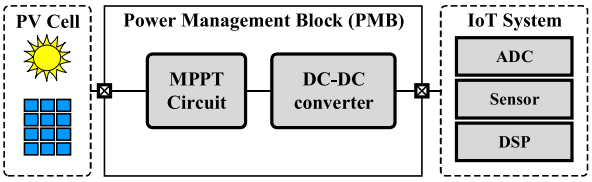

FIGURE 1. DC energy harvesting systems.

The associate editor coordinating the review of this manuscript and approving it for publication was Sze Sing Lee.

used to provide maximum efficient extracted power to the load and it ensures that the EHS always operates at its MPP. Several MPPT methods have been studied and they can be classified into two categories, direct MPPT and indirect MPPT. In the direct MPPT algorithm, extracted power of the PV cells is directly sensed and tracked by controlling the internal signal of the DC-DC converter accordingly. The simple example is the Perturbation and Observation (P&O) scheme [18], [19]. In this scheme, the extracted power is periodically estimated by measuring the output voltage and current, and is compared with the previous extracted power level. Then, the comparison result is used to control the MPPT circuit. Although the direct MPPT is an intuitive approach, the system suffers from the need to continuously monitor the extracted power of the PV cells using a built-in voltage and current sensor. Due to the power consumption issue, it is not suitable for ultra-low-power IoT systems. To solve this problem, the researchers have studied indirect MPPT algorithms that can estimate the extracted power without using the sensors. Among them, Time-Based MPPT (TB-MPPT), a technology that monitors the timing information of DC-DC converters, is commonly used. For example, the extracted power can be estimated by measuring the pulse width of the power switch [3]. This algorithm alleviates the power consumption problem, but one of the drawbacks is that the MPPT circuit oscillates near the MPP, resulting in reduced power tracking efficiency.

In order to solve the oscillation problem and reduce the hardware overhead (power and chip area), this article proposes a highly efficient TB-MPPT method which is mainly performed through digital blocks. The proposed scheme is based on a hill climbing algorithm with two-period tracking operations and convergence range averaging technique.

This article is organized as follows. Session II describes the operation of the conventional TB-MPPT, along with key design parameters, and discusses the performance limitations. Then, the proposed scheme will be presented in Section III. The overall architecture and circuit-level implementation of the proposed TB-MPPT circuit are presented in Section IV. Section V shows the measured performance and comparison results with previous state of arts. Finally, the conclusion is given in Section VI.

II. TB-MPPT CIRCUIT

A. GENERAL PRINCIPLE OPERATION OF TB-MPPT CIRCUIT

Fig. 2 shows the block diagram of the previous EHS with TB-MPPT circuit [3]. The TB-MPPT circuit must match the impedance of DC-DC converter with output impedance of PV cell to extract maximum power. The impedance of DC-DC converter can be expressed as

$$\frac{V_{PV}}{I_{PV}} \approx \frac{2.L}{t_1^2.f_s} \tag{1}$$

where the V_{PV} and I_{PV} are the output voltage and current of the PV cell, L is the inductor inside the converter, t_1 is

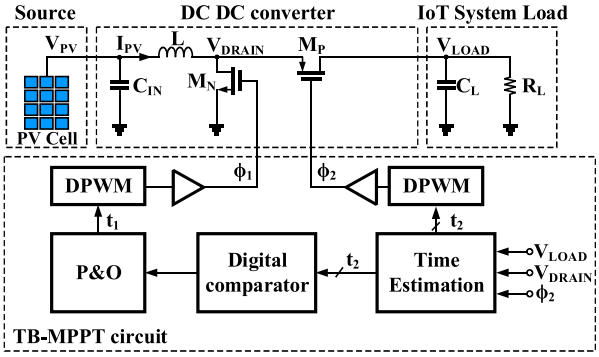

FIGURE 2. Block diagram of previous EHS with TB-MPPT circuit.

time information of ϕ_1, and f_s is the switching frequency. As we can see from (1), the impedance of DC-DC converter (V_{PV}/I_{PV}) is inversely proportional to the t_1, and this shows that the extracted power could be tracked by adjusting the t_1. In addition, the extracted power is strongly related to the time information of ϕ_2 as the following equation

$$t_2 = \frac{1}{V_{LOAD}} \cdot \sqrt{\frac{2.L.P_{PV}}{f_s}} \tag{2}$$

where t_2 is time information of ϕ_2, V_{LOAD} is output voltage of DC-DC converter, P_{PV} is extracted power from PV cell. In the ideal case, V_{LOAD}, f_s, and L are constant. Hence, the P_{PV} is directly proportional to t_2 and P_{PV} could be estimated by measuring the t_2. Even though the parameters t_1 and t_2 are explained separately from the (1) and (2), those parameters are closely related to each other. Once the impedance of the DC-DC converter is tuned by adjusting the t_1, the P_{PV} will be affected. Then, the system could detect the changes in P_{PV} by monitoring t_2, and tries to track the MPP by changing the t_1. This closed-loop fashion control continues until the MPP is tracked. The TB-MPPT operation is as follows. Firstly, the 'Time Estimation' block compares the voltage at V_{LOAD} and V_{DRAIN} nodes to properly decide the t_2. This block follows the Zero-Current Switching (ZCS) algorithm which will be explained in detail in Section IV-B. The t_2 will be sent to both 'DPWM' (Digital Pulse Width Modulator) and 'Digital Comparison' blocks. In 'DPWM', t_2 is converted into control pulse ϕ_2 that turns the M_P on and off. And the 'Digital Comparison' block compares the current and previous t_2 to see if there is any change in the timing information. This operation determines the tracking direction of the 'P&O' block that will eventually control the pulse width of the M_N signal (ϕ_1). By repeating this tracking procedure, the MPP could be found. Then, the DC-DC converter provides extracted power to the load.

B. LIMITAION OF PREVIOUS TB-MPPT CIRCUIT

The previous TB-MPPT is useful because the extracted power and impedance of DC-DC converter are expressed in time domain information. This simplifies the circuit as it can be implemented using digital circuit. However, the closed-loop feedback based on hill-climbing progresses

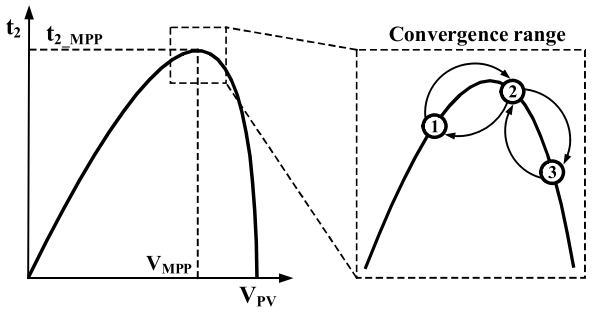

FIGURE 3. Visualization of oscillation problem of previous TB-MPPT.

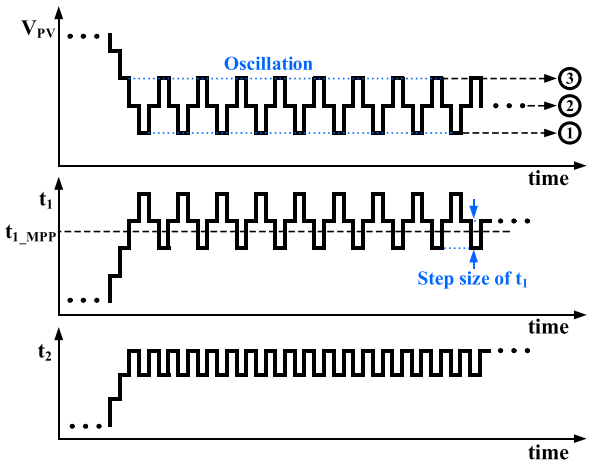

FIGURE 4. Timing diagram of previous TB-MPPT.

shows an oscillation near MPP as shown in Fig. 3. Initially, there is no power transfer to the load side. When the power transfer reaches its MPP, the system oscillates without staying at the MPP. In particular, three tracking points are existing around the MPP. The tracking point '1' and '3' are far from the MPP compared to '2'. This makes the extracted power from PV cell degrades and the overall performance of the TB-MPPT circuit will also be deteriorated. Based on our estimation, this oscillation problem lowers the overall power transfer by 6%-7%. In addition, according to (2), the t_2 is not strictly proportional to P_{PV}. Due to the voltage ripples occurring at the V_{LOAD} node, t_2 fluctuates and therefore the tracking operation does not perform the desired behavior. To alleviate this issue, a large t_1 step could be considered. But the oscillation problem worsens once the unit step of the t_1 becomes large as the tracking system moves the tracking point far from the MPP during the oscillation as shown in Fig. 4. Any single step in t_1 could make a change in t_2. Therefore, careful consideration is required to determine the appropriate step size for both t_1 and t_2.

III. PROPOSED TB-MPPT CIRCUIT

As mentioned in the Section II, there are two possible spots that could be improved for the overall power transfer performance. First, the system parameters (especially t_1 and t_2) should be fixed at MPP (or near-MPP) to solve the oscillation problem. Also, the unit step size of t_1 and t_2 has to be decided

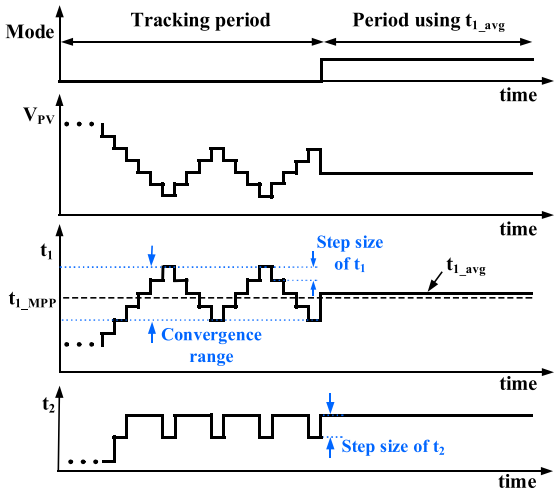

FIGURE 5. Proposed TB-MPPT circuit timing diagram.

carefully to prevent an unwanted fluctuation on the t_2 and also for accurate tracking process. To achieve the first goal, finding the MPP without oscillation, we adopted a convergence range averaging technique that finds the mean value of t_1 over a period of time. The idea behind this technique arises from the fact that the MPP is close to the middle point of convergence range, i.e., the average value of t_1 over a certain period time. Fig. 5 illustrates how to determine the steps of t_1 through the hill-climbing process. Initially, the system starts from the left-most step with the minimum t_1 value. Since the t_1 is not large enough, the system increases t_1 by a unit step and eventually reaches the MPP at t_{1_MPP}. Once the t_1 value goes beyond the t_{1_MPP}, the system still continues to move the t_1 such that tracking system requires a reverse change in t_2. The system rather toggles the direction of change in t_1 at the step where the t_1 is at the top of the convergence range. A similar movement would happen when the system moves t_1 value back to the t_{1_MPP} again. Once this repeated behavior happens during the MPP tracking operation, the value of t_1 near the MPP will mostly happen throughout the tracking process. Then, the MPP could be approximated by taking the average value of t_1 (t_{1_avg}) during the tracking period. To measure the average value, we employ the 'Digital Average' block and make the system use the t_{1_avg} after tracking period such that no further oscillation happens. Note that, to get accurate tracking point, fine granularity of t_1 is desirable as the t_{1_avg} will have a small gap to the MPP. In this scenario, if t_1 and t_2 are having the same step size, then the fine t_1 step also means a small step for t_2. Hence, a small voltage ripples on the V_{LOAD} node affect the changes in t_2 more frequently with a fine t_2 step. On the other hand, there is a possibility of having a large convergence range once the t_2 would have a fine step which leads to less-optimal average value for MPP. To prevent these issues, our proposed TB-MPPT circuit has adaptive step size for t_1 and t_2. In particular, the t_2 shows a single transition whereas the t_1 code changes several steps in convergence range. To find the optimum step size of t_1, we check the gap between t_{1_avg} and the t_{1_MPP} at different unit step size of t_1 as shown in Fig. 6. Obviously, with a coarse t_1 step, the t_{1_avg}

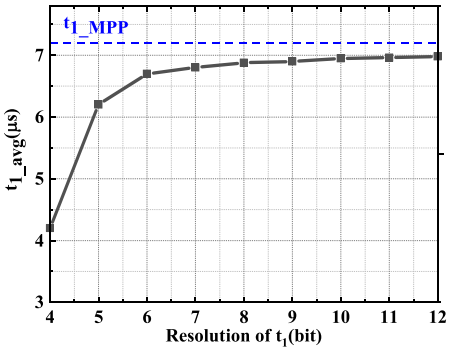

FIGURE 6. Consideration of time resolution of t_1.

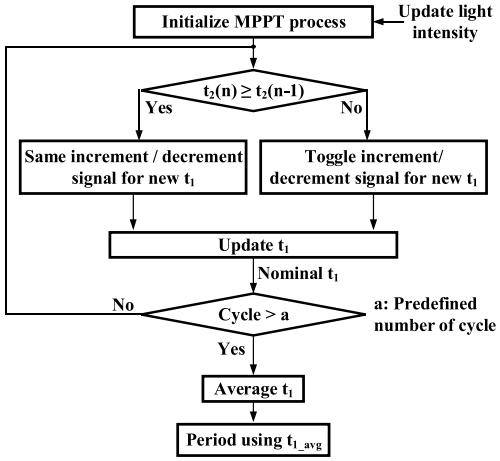

FIGURE 7. Proposed TB-MPPT circuit flow chart.

is far from the t_{1_MPP}. When the t_1 step becomes around 50ns, the system is saturated near the MPP and this corresponds to the 8-bit resolution. Based on this characterization, we have chosen an 8-bit resolution of t_1 for our proposed TB-MPPT circuit.

The overall operation flow of the proposed TB-MPPT algorithm is illustrated in Fig. 7. Once the system starts operation, the current extracted power information 't_2(n)' is compared to the previous one 't_2(n-1)' to check if extracted power has been changed. Depending on the comparison results, the controller on the t_1 side determines the change direction of t_1. Regardless of the changes of t_2 in the current stage, the selected code for t_1 is monitored and recorded using an additional logic so that the system can define the t_{1_avg} for the predefined number of cycles. In our work, the system repeats this update process until the number of cycles reaches 256 times. Then, the t_{1_avg} will be calculated and applied to the system. At this stage, the system holds the t_{1_avg} which is the optimal tracking point. Note that, the system periodically repeats this tracking process to update the MPP even with an environmental change such as light intensity variation.

IV. CIRCUIT IMPLEMENTATION

A. OVERALL ARCHITECTURE

The overall block diagram of the EHS with proposed TB-MPPT circuit is shown in Fig. 8. The basic components of the system, such as PV cell, DC-DC converter,

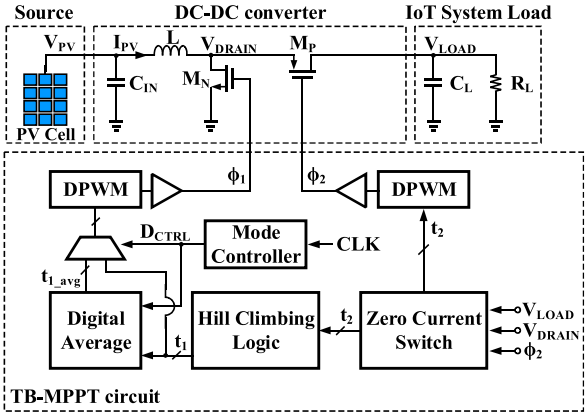

FIGURE 8. Block diagram of EHS with proposed TB-MPPT circuit.

and the RC load are maintained to be the same as the conventional system. Instead, many functional blocks (Mode Controller, 2:1 MUX, and Digital Average) are added inside the TB-MPPT block to handle the oscillation problem. Note that, the 'Time Estimation' and 'Digital Comparison' blocks from Fig. 2 are renamed as 'Zero Current Switch' (ZCS) and 'Hill Climbing Logic' (HCL) with a proper modification inside. The basic operation of the proposed TB-MPPT circuit including the additional logics for the convergence range averaging technique can be explained as follows. The ZCS first determines a time duration t_2 based on the level comparison between incoming voltages from V_{LOAD} and V_{DRAIN} node. The t_2 is converted into a pulse through the 'DPWM' before presenting to the M_P. At the same time, t_2 is also provided to the HCL to update the t_1 as a part of the MPP tracking process. The basic idea of the tracking process in HCL is simple. Depending on whether extracted power level reflected in t_2 is larger or equal (smaller) than the previous level stored in memory, the HCL keeps (inverts) the current tracking direction and updates t_1 by a unit step. Corresponding t_1 value is fed into the 'Digital Average' and 'MUX'. In the 'Digital Average' block, the incoming t_1 code is accumulated for a certain period to take the t_{1_avg}. If the 'Digital Average' block outputs the t_{1_avg}, the 'MUX' passes the t_{1_avg} from the 'Digital Average' to the 'DPWM'. Otherwise, the 'DPWM' uses nominal t_1 value directly from the HCL unit. The changes in t_1 value represent that the effective impedance of the DC-DC converter is changing to find the MPP under the current system environment. The overall operation flow with estimated waveforms is shown in Fig. 9. In Fig. 9(a), the voltage variation on V_{PV} node during tracking period and period using t_{1_avg} are shown depends on the state of the D_{CTRL} signal. Note that, here the D_{CTRL} signal indicates that the system is under tracking period (or average evaluation period) during the signal has low state. The system averages t_1 code for 256 times, then the D_{CTRL} signal shows a transition to high once the average calculation is done. Then the system uses t_{1_avg} which is close to MPP point. The t_{1_avg} is used for a certain period of time based on the system timing controller. After 256 cycles, the system forces D_{CTRL} code

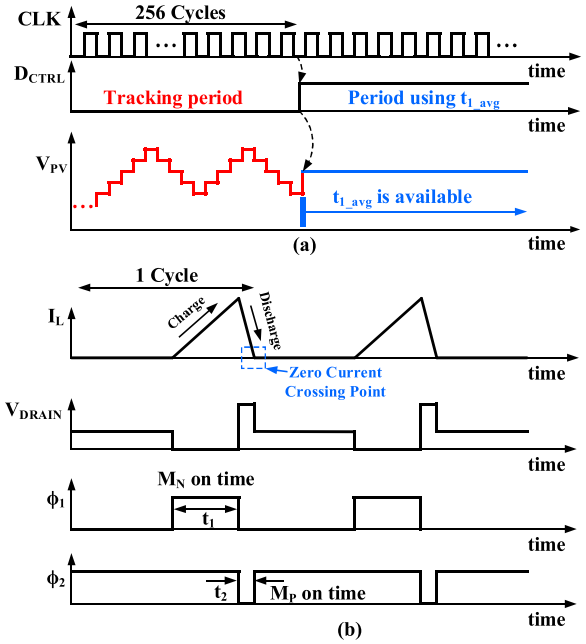

FIGURE 9. (a) Timing diagram of proposed MPPT circuit, (b) 1 switching cycle ZCS waveform.

to low such that environmental variation could be tracked to update the MPP. The Fig. 9(b) shows the DC-DC converter waveforms at steady state. Specifically, the relation between ϕ_1 and ϕ_2, also the corresponding inductor current flow (I_L) are shown. The I_L is charged when the M_N is turned on (ϕ_1 = high) and discharged when the M_P is turned on (ϕ_2 = low). The ZCS unit determines the zero current crossing point and turns the M_P off to prevent losing power.

B. ZERO-CURRENT SWITCH (ZCS)

The ZCS is used as a power monitor part of the tracking loop in the proposed TB-MPPT circuit. It is targeted for preventing losing power due to the zero current detection timing issues. The basic idea of its operation comes from the inductor-volt second and t_2 would have the relation defined below

$$t_2 = \frac{V_{PV}.t_1}{V_{LOAD} - V_{PV}} \tag{3}$$

In this relation, both the voltages V_{PV} and V_{LOAD} are the variables that restrict the usage of open-loop ZCS. Instead, closed-loop ZCS [14] could be exploited in this design and its implementation is illustrated in Fig. 10. Here the upper part describes a DC-DC converter and load side schematic to show the connection between main timing signal (ϕ_1, ϕ_2) and the ZCS part. As mentioned in the previous section, the t_1 represents the time duration of the M_N, and it is generated from HCL that utilizes the t_2 from the ZCS. To achieve the ZCS operation, the t_2 needs to follow the relation in (3). Since this equation shows the relation between t_1 and t_2 with respect to two voltage levels across the M_P, the ZCS operation could be implemented by comparing the voltages at V_{DRAIN} with V_{LOAD} nodes immediately after the M_P is turned off. In case the M_P is turned off too quickly, this means the current t_2

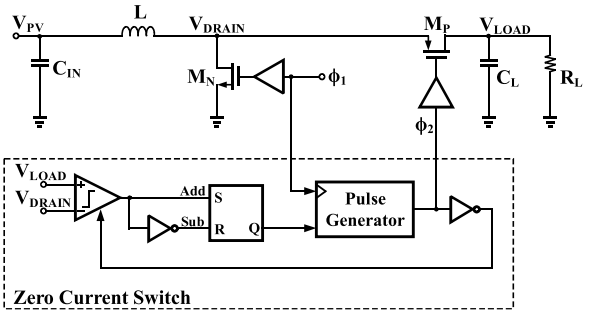

FIGURE 10. Schematic of ZCS.

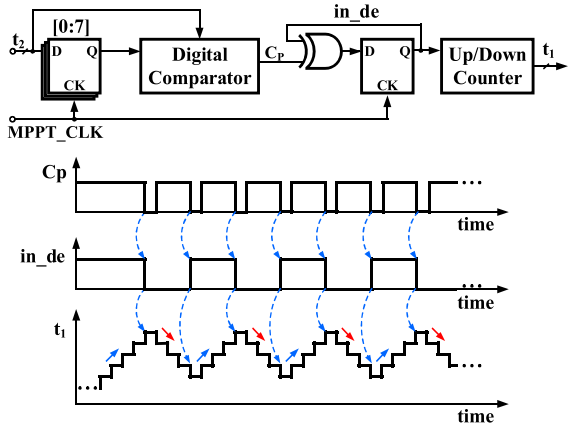

FIGURE 11. Schematic of HCL and its timing diagram during tracking period.

is shorter than the required value and the remaining inductor current in L turns on the parasitic diode across the M_P. This forces the voltage at V_{DRAIN} go to beyond the V_{LOAD} level. On the other hand, if the M_P is turned off too late (if t_2 is longer than needed), the inductor current reverses direction and the voltage level at V_{DRAIN} node goes below the V_{LOAD} level, and even becomes lower than zero. To find the optimum timing, a simple feedback logic could be utilized to determine the proper value of t_2 by comparing the V_{DRAIN} and V_{LOAD}. The bottom block diagram of the figure shows the actual implementation of the ZCS part. The comparator at the beginning stage receives voltages from V_{DRAN} and V_{LOAD} nodes and determines whose level is higher. If V_{DRAIN} is higher (lower) than V_{LOAD}, only the Add (Sub) pulse goes high. This makes the output from SR latch high (low). Depending on the level of SR latch output, the 'Pulse Generator' increases (decreases) the t_2 by a single step. This process is repeated to achieve zero current crossing point of the inductor current.

C. HILL CLIMBING LOGIC (HCL)

The output from ZCS part (t_2) is presented to HCL and is used to determine the perturbation direction in t_1 in the next time step. Fig. 11 shows the schematic of HCL and the corresponding expected waveforms during tracking period. Once the current power information in t_2 is sent to the 'Digital Comparator' block, the previous t_2 code is stored in D-Flip Flops. The comparison result (C_P) is used to control

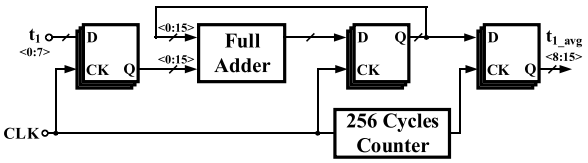

FIGURE 12. Schematic of digital average block.

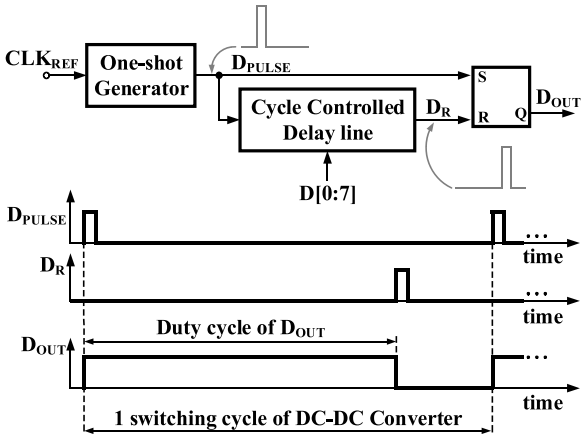

FIGURE 13. Schematic of DPWM and its timing diagram.

the perturbation direction of t_1, which is denoted as 'in_de' signal. Here the logic is rather simple, if the current extracted power level is greater than or equal to the previous level, then C_P becomes logic high. Then t_1 keep moving in the same direction. Otherwise, the direction of perturbation is reversed using the XOR gate, since the C_P is low. Finally, t_1 is increased or decreased by a unit time step, according to the polarity of the 'in_de' signal from the 'Up/Down Counter'.

D. DIGITAL AVERAGE BLOCK

The Digital Average block is used to estimate the average time duration of t_1 over 256 iterations. We have used an averaging technique based on chopping LSB data after accumulating 256 times of t_1 to reduce the power and silicon area overhead. Note that, the 8-bit time resolution of t_1 is used based on the case study in Section III. The schematic of the 'Digital Average' block is shown in Fig. 12. The t_1 is summed up using a full adder for 256 cycles during tracking period. Here the '256 Cycles Counter' monitors the number of cycles passed during the accumulation period and makes the 'Digital Average' stop accumulating to generate the average value. Once the number of collected cycles reaches 256 times, the 'Full Adder' is being reset and the t_{1_avg} is simply estimated by taking the first 8 bits of the output from 16-bit full-adder as mentioned. This simple method contributes to comparable power consumption of the proposed TB-MPPT system as compared to the previous works.

E. DPWM BLOCK

The DPWM block gets the time information (t_1, t_2) from the previous stage and converts this into the pulse whose width is proportional to the incoming code. Fig. 13 shows the simplified block diagram of the DPWM [20]. Initially, the 'Once-shot Generator' is used to generate a pulse (D_{PULSE}) which maintains logic high for a short duration. This short pulse prevents both inputs of the next SR latch from being enabled to logic high at the same time. The rising edge of D_{PULSE} sets the SR latch output (Q) to logic high. Meanwhile, D_{PULSE} goes through the 'Cycle Controlled Delay Line' and being delayed by the amount dictated from the incoming code D [0:7]. The rising edge of delayed pulse (D_R) resets the SR latch to logic low. Hence, the duty cycle of D_{OUT} can be expressed as

$$\text{Duty cycle of } D_{OUT} = \frac{t_{delay}}{t_{period}}.100\% \quad (4)$$

where the t_{delay} is distance from rising edge of D_{PULSE} to rising edge of D_R, and t_{period} is 1 switching cycle of DC-DC converter. The t_{delay} is adjustable using the 8-bit code, D [0:7].

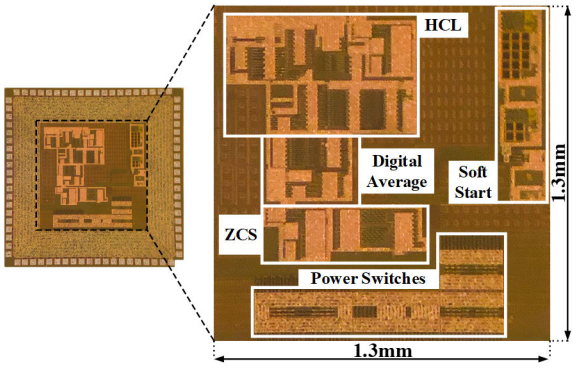

FIGURE 14. Die photo.

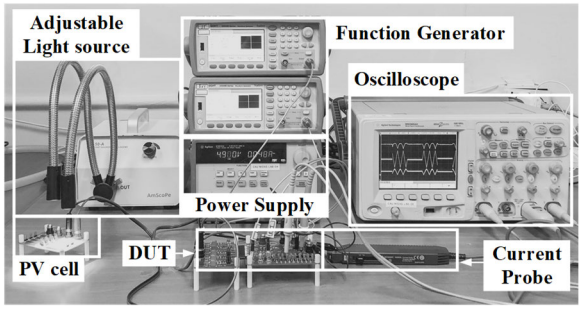

FIGURE 15. Measurement setup.

V. MEASUREMENT RESULTS AND COMPARISONS

The proposed TB-MPPT circuit along with a DC-DC converter was implemented in 180 nm CMOS process. Fig. 14 shows the die photo of the fabricated chip where the active area of the proposed chip is 1.3mm x 1.3mm. The majority of the area is occupied by the power switches and HCL. Fig. 15 shows the measurement setup for EHS where a halogen lamp is used as an adjustable light source. We first monitored the time duration of ϕ_1 and ϕ_2, i.e. t_1 and t_2, and also the performance of the ZCS logic. We chose the time resolution for t_1 as 50ns and the proposed system harvests the energy from a 7×22 mm^2 PV cell. The resultant

TABLE 1. Comparison with prior arts.

	JSSC [3] 2012	JSSC [7] 2013	JSSC [6] 2016	ISSCC [21] 2018	**This work**
Technology	350nm	190nm	350nm	28nm	**180nm**
MPPT method	Indirect MPPT	Fractional Open-circuit	Direct MPPT	Direct MPPT	**Indirect MPPT**
Energy sources	Photovoltaic, Thermoelectric and Vibration	Photovoltaic	Photovoltaic	Photovoltaic Thermoelectric and Biofuel	**Photovoltaic**
Input voltage to power converters	0.15-0.75V Photovoltaic	1V	10-43V	0.2 – 1V Photovoltaic	**0.47V**
Switching frequency	31.25KHz	330KHz	1MHz	Adaptive frequency 40KHz-500KHz	**30KHz**
In-build Maximum Power Extraction	Yes	No	Yes	Yes	**Yes**
Peak Tracking Efficiency for Photovoltaic	96% (Oscillation)	N/A	94.2%	N/A	**94.2% (No oscillation)**
Maximum Output Power	10mW	N/A	21W	60mW	**12mW**
Peak Efficiency of power converters	87%	87%	99.9%	89%	**91.6%**
Chip area	25mm^2	0.75mm^2	8.1mm^2	0.5mm^2	**1.69mm^2**

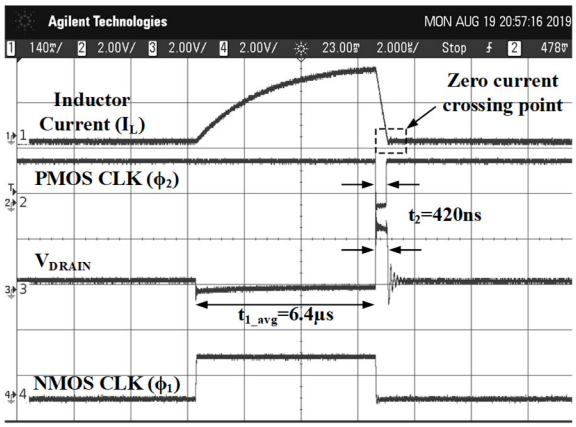

FIGURE 16. Zero current switch waveform.

waveforms are shown in Fig. 16. The measured t_1 and t_2 show 6.4μs and 420ns of time duration, respectively. Regarding the performance of ZCS logic, we have drawn a dashed box on the waveform of inductor current (I_L) at the top. This point is followed by the sharp decrease of the I_L during ϕ_2 is low. As shown inside the box, there is no upward or downward peaking and it is exactly showing zero-level at the end of ϕ_2 which means our ZCS logic works as intended. The MPP tracking performances under various light conditions and shading condition are shown in Fig. 17. To emulate indoor illumination, various light intensities of 400, 600, and 800 lux were used. Fig. 17(a, b, and c) show the tracking performance under different light intensities where the blue dashed line at the top shows the maximum extracted power level (P_{MPP}). As can be seen from the figure, once the proposed MPPT circuit uses t_{1_avg}, the extracted power (P_{PV}) reaches 6mW, 8.67mW, and 11.3mW which results in 91.2%, 92.2%, and 94.2% of tracking efficiency, respectively. Our convergence range averaging technique during the tracking process is also shown in all the waveforms where there is some repeated behavior during the tracking period and after that, the waveform shows a steady state near the MPP without oscillation that might cause efficiency degradation in the previous approach [3]. Fig. 17(d) shows the performance of the proposed MPPT circuit under shading condition. As we can see, the MPPT circuit can return to normal condition after being interrupted. The dynamic tracking performance of the proposed system is also evaluated by varying the light intensity from the initial value as shown in Fig. 17(e, f). The two light intensities of 600 lux and 800 lux were used in this evaluation. The proposed MPPT circuit is capable of tracking light intensity transitions in real-time and extracts the maximum power immediately. The V_{PV} shows a gradual change from 470mV (@800 lux) to 450mV (@600 lux), and

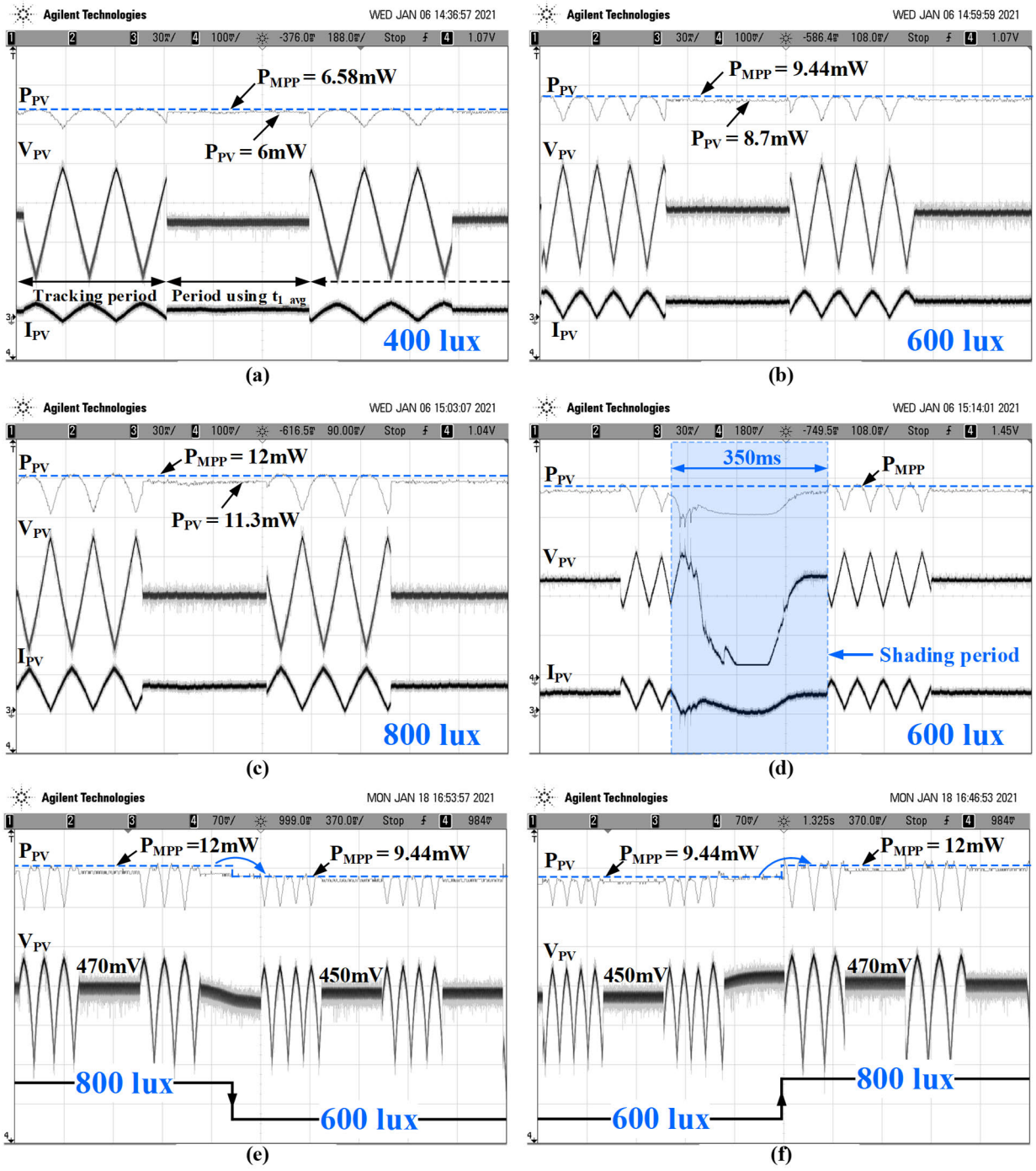

FIGURE 17. MPP tracking performance of proposed TB-MPPT circuit under (a) 400, (b) 600, (c) 800 lux conditions, (d) Shading condition, (e) Transition from 800 to 600 lux, (f) Transition from 600 to 800 lux.

vice versa. This confirms that the operation of the proposed system is consistent under different conditions. Before moving on the comparison table, let us briefly mention the power consumption analysis of the proposed system. Start from the previous TB-MPPT circuit with a hill-climbing algorithm, the two periods tracking algorithm and convergence range averaging technique have been adopted for the efficient MPP finding. As can be seen from Fig. 18, the power consumption of HCL including the additional digital logics just occupies 2% of total power. Regarding the detailed power number, the entire power consumption of the system is 0.95mW, where the Power Switches and Buffer part consume most of the power, 69%. The ZCS, and DPWM consume 18%, and 11%, respectively. Based on these power numbers, the power conversion efficiency turns out to be 91.6%. Finally, Table. 1 shows a comparison between the previous state of arts and

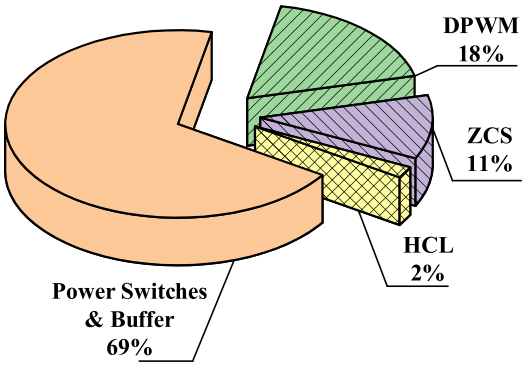

FIGURE 18. Detail power consumption of the proposed EHS.

the proposed system. All the PV systems except the work in [6] target low-power PV systems and harvest less than tens of mW from sources. Concerning the peak tracking efficiency for PV cell, the work in [6] shows a similar level of efficiency to our work, whereas peak efficiency of power converter reaches up to 99.9%. These superiorities are due to the fact that the system in [6] targeted a high-power PV system where the power consumption of the MPPT circuit can be neglected in comparison to the total power of the EHS. On the other hand, the peak tracking efficiency from [3] is slightly higher than our proposal, but, the number in [3] is obtained from taking the closest point to MPP where the two other points are far from the MPP during steady state. As the proposal from [3] naturally has an oscillation problem near the MPP, we are expecting that the peak tracking efficiency would show some drop from the maximum point. In conclusion, the proposed TB-MPPT circuit for DC-DC converter shows a good accuracy in both peak tracking and power conversion whereas consuming a reasonable power in comparison to the other works targeting similar applications.

VI. CONCLUSION

This work proposes a TB-MPPT circuit for DC-DC converter which utilizes a PV cell as an energy source. The proposed circuit solves the oscillation problem of the previous work by exploiting the two-period tracking algorithm and convergence range averaging technique with an adaptive perturbation step. Based on the circuit techniques we proposed, peak tracking efficiency of the system has been increased by ∼7% whereas the additional power consumption is less than 2% of the total power budget. The test chip was implemented in 180 nm technology, and achieves the tracking accuracy of 94.2% and the conversion efficiency of 91.6%.

REFERENCES

[1] K. Rawy, T. Yoo, and T. T.-H. Kim, "An 88% efficiency 0.1–300-μ W energy harvesting system with 3-D MPPT using switch width modulation for IoT smart nodes," *IEEE J. Solid-State Circuits*, vol. 53, no. 10, pp. 2751–2762, Oct. 2018.

[2] X. Liu and E. Sanchez-Sinencio, "21.1 A single-cycle MPPT charge-pump energy harvester using a thyristor-based VCO without storage capacitor," in *IEEE Int. Solid-State Circuits Conf. (ISSCC) Dig. Tech. Papers*, Jan. 2016, pp. 364–365.

[3] S. Bandyopadhyay and A. P. Chandrakasan, "Platform architecture for solar, thermal, and vibration energy combining with MPPT and single inductor," *IEEE J. Solid-State Circuits*, vol. 47, no. 9, pp. 2199–2215, Sep. 2012.

[4] K. Rawy, F. Kalathiparambil, D. Maurath, and T. T.-H. Kim, "A self-adaptive time-based MPPT with 96.2% tracking efficiency and a wide tracking range of 10 μ a to 1 mA for IoT applications," *IEEE Trans. Circuits Syst. I, Reg. Papers*, vol. 64, no. 9, pp. 2334–2345, Sep. 2017.

[5] K. Rawy, F. K. George, D. Maurath, and T. T. Kim, "A time-based self-adaptive energy-harvesting MPPT with 5.1-μW power consumption and a wide tracking range of 10-μA to 1-mA," in *Proc. Conf., 42nd Eur. Solid-State Circuits Conf. (ESSCIRC)*, Sep. 2016, pp. 503–506.

[6] S. Uprety and H. Lee, "A 0.4W-to-21W fast-transient global-search-algorithm based integrated photovoltaic energy harvester with 99% GMPPT efficiency and 94% power efficiency," *IEEE J. Solid-State Circuits*, vol. 51, no. 9, pp. 2153–2167, Sep. 2016.

[7] Y. Nakase, S. Hirose, H. Onoda, Y. Ido, Y. Shimizu, T. Oishi, T. Kumamoto, and T. Shimizu, "0.5 v start-up 87% efficiency 0.75 mm^2 on-chip feed-forward single-inductor dual-output (SIDO) boost DC-DC converter for battery and solar cell operation sensor network micro-computer integration," *IEEE J. Solid-State Circuits*, vol. 48, no. 8, pp. 1933–1942, Aug. 2013.

[8] X. Liu and E. Sanchez-Sinencio, "An 86% efficiency 12 μW self-sustaining PV energy harvesting system with hysteresis regulation and time-domain MPPT for IOT smart nodes," *IEEE J. Solid-State Circuits*, vol. 50, no. 6, pp. 1424–1437, Jun. 2015.

[9] O. Lopez-Lapena, M. T. Penella, and M. Gasulla, "A closed-loop maximum power point tracker for subwatt photovoltaic panels," *IEEE Trans. Ind. Electron.*, vol. 59, no. 3, pp. 1588–1596, Mar. 2012.

[10] H. Kim, S. Kim, C.-K. Kwon, Y.-J. Min, C. Kim, and S.-W. Kim, "An energy-efficient fast maximum power point tracking circuit in an 800-μW photovoltaic energy harvester," *IEEE Trans. Power Electron.*, vol. 28, no. 6, pp. 2927–2935, Jun. 2013.

[11] X. Liu, L. Huang, K. Ravichandran, and E. Sanchez-Sinencio, "A highly efficient reconfigurable charge pump energy harvester with wide harvesting range and two-dimensional MPPT for Internet of Things," *IEEE J. Solid-State Circuits*, vol. 51, no. 5, pp. 1302–1312, May 2016.

[12] O. Lopez-Lapena, M. T. Penella, and M. Gasulla, "A new MPPT method for low-power solar energy harvesting," *IEEE Trans. Ind. Electron.*, vol. 57, no. 9, pp. 3129–3138, Sep. 2010.

[13] J. Li, J.-S. Seo, I. Kymissis, and M. Seok, "Triple-mode, hybrid-storage, energy harvesting power management unit: Achieving high efficiency against harvesting and load power variabilities," *IEEE J. Solid-State Circuits*, vol. 52, no. 10, pp. 2550–2562, Oct. 2017.

[14] Y. K. Ramadass and A. P. Chandrakasan, "A battery-less thermoelectric energy harvesting interface circuit with 35 mV startup voltage," *IEEE J. Solid-State Circuits*, vol. 46, no. 1, pp. 333–341, Jan. 2011.

[15] J. Leicht, M. Amayreh, C. Moranz, D. Maurath, T. Hehn, and Y. Marioli, "20.6 Electromagnetic vibration energy harvester interface IC with conduction-angle-controlled maximum-power-point tracking and harvesting efficiencies of up to 90%," in *IEEE Int. Solid-State Circuits Conf. (ISSCC) Dig. Tech. Papers*, Feb. 2015, pp. 1–3.

[16] S.-Y. Kim, H. Abbasizadeh, B. S. Rikan, S. J. Oh, B. G. Jang, Y.-J. Park, D. Khan, T. T. K. Nga, K. T. Kang, Y. G. Pu, S.-S. Yoo, S. Lee, S.-C. Lee, M. Lee, K. C. Hwang, Y. Yang, and K.-Y. Lee, "A −20 to 30 dBm input power range wireless power system with a MPPT-based reconfigurable 48% efficient RF energy harvester and 82% efficient A4WP wireless power receiver with open-loop delay compensation," *IEEE Trans. Power Electron.*, vol. 34, no. 7, pp. 6803–6817, Jul. 2019.

[17] Z. Zeng, S. Shen, X. Zhong, X. Li, C.-Y. Tsui, A. Bermak, R. Murch, and E. Sanchez-Sinencio, "Design of sub-gigahertz reconfigurable RF energy harvester from −22 to 4 dBm with 99.8% peak MPPT power efficiency," *IEEE J. Solid-State Circuits*, vol. 54, no. 9, pp. 2601–2613, Sep. 2019.

[18] N. Femia, G. Petrone, G. Spagnuolo, and M. Vitelli, "Optimization of perturb and observe maximum power point tracking method," *IEEE Trans. Power Electron.*, vol. 20, no. 4, pp. 963–973, Jul. 2005.

[19] S. Jain and V. Agarwal, "A new algorithm for rapid tracking of approximate maximum power point in photovoltaic systems," *IEEE Power Electron Lett.*, vol. 2, no. 1, pp. 16–19, Mar. 2004.

[20] W.-C. Chen, C.-C. Chen, C.-Y. Yao, and R.-J. Yang, "A fast-transient wide-voltage-range digital-controlled buck converter with cycle-controlled DPWM," *IEEE Trans. Very Large Scale Integr. (VLSI) Syst.*, vol. 24, no. 1, pp. 17–25, Jan. 2016.

[21] S. S. Amin and P. P. Mercier, "MISIMO: A multi-input single-inductor multi-output energy harvester employing event-driven MPPT control to achieve 89% peak efficiency and a 60,000x dynamic range in 28 nm FDSOI," in *IEEE Int. Solid-State Circuits Conf. (ISSCC) Dig. Tech. Papers*, Feb. 2018, pp. 144–146.

VAN-THAI DANG (Student Member, IEEE) received the B.S. degree from the School of Electronics and Communications Engineering, Hanoi University of Industry (HAUI), Hanoi, Vietnam, in 2013, and the M.S. degree in electrical and electronics engineering from Chung-Ang University, Seoul, South Korea, in 2018, where he is currently pursuing the Ph.D. degree in electrical and electronic engineering.

He was a member with the Research and Development Group, Samsung Electronics Vietnam, from 2013 to 2016. His current research interests include mixed-signal integrated circuit design, low-power dc–dc converter, and energy harvesting systems.

MYEONG-GYU YANG (Student Member, IEEE) received the B.S. degree from the School of Electrical and Electronics Engineering, Chung-Ang University, Seoul, South Korea, in 2020, where he is currently pursuing the M.S. degree in electrical and electronic engineering.

His current research interests include mixed-signal integrated circuit design, switched-capacitor dc–dc converter, and energy harvesting systems.

YONG SHIM (Member, IEEE) received the B.S. and M.S. degrees in electronics engineering from Korea University, in 2004 and 2006, respectively, and the Ph.D. degree from the School of Electrical and Computer Engineering, Purdue University, West Lafayette, IN, in 2018. He was a Memory Interface Designer with Samsung Electronics, Hwasung, from 2006 to 2013. At Samsung, he has worked on the design and development of a memory interface for synchronous DRAMs (DDR1 and DDR4). He is currently an Assistant Professor with Chung-Ang University. Prior to joining Chung-Ang University, in 2020, he was an SRAM Designer with Intel Corporation, Hillsboro, OR, from 2018 to 2020, where he was involved in designing circuits for super-scaled next-generation SRAM cache design. His research interests include neuromorphic hardware and algorithm, in-memory computing, robust memory interface design, as well as emerging devices (RRAM, MRAM, and STO) based unconventional computing models.

WOOJOO LEE (Member, IEEE) received the B.S. degree in electrical engineering from Seoul National University, Seoul, South Korea, in 2007, and the M.S. and Ph.D. degrees in electrical engineering from the University of Southern California, Los Angeles, CA, in 2010 and 2015, respectively. From 2015 to 2016, he was a Senior Researcher with the SoC Design Research Group, Electronics and Telecommunications Research Institute, Daejeon, South Korea. From 2017 to 2018, he was an Assistant Professor with the Department of Electrical Engineering, Myongji University, Yongin, South Korea. He is currently an Assistant Professor with the School of Electrical and Electronics Engineering, Chung-Ang University, Seoul. His research interests include ultra-low power VLSI and SoC designs, embedded system designs, and system-level power and thermal management.

KWANG-HYUN BAEK (Senior Member, IEEE) received the B.S. and M.S. degrees from Korea University, Seoul, South Korea, in 1990 and 1998, respectively, and the Ph.D. degree in electrical engineering from the University of Illinois at Urbana–Champaign (UIUC), IL, USA, in 2002. From 2000 to 2006, he was the Senior Scientist of the Department of High-Speed Mixed-Signal ICs, Rockwell Scientific Company, formerly the Rockwell Science Center (RSC), Thousand Oaks, CA, USA. At RSC, he was involved in development of high-speed data converters (ADC/DAC) and direct digital frequency synthesizers (DDFS). He was also with Samsung Electronics, from 1990 to 1996. Since 2006, he has been with the School of Electrical and Electronics Engineering, Chung-Ang University (CAU), Seoul, where he is currently a Faculty Member. His research interests include high-performance analog and digital circuits, such as low-power ADCs, high-speed DACs, hybrid frequency synthesizers (PLLs and DDFSs), high-speed interface circuits (CDRs and SerDes), PMIC, and near threshold-voltage (NTV) circuits.